Theoretical Study of Above-Threshold Dissociation on Diatomic Molecules by Using Nonresonant Intense Laser Pulses†

Kimikazu Sugimori,*,‡ Tomoya Ito,§ Yusuke Takata,§ Kazuhiro Ichitani,§ Hidemi Nagao,§ and Kiyoshi Nishikawa§

Kinjo University, Kasama, Hakusan 924-8511, Japan, and Division of Mathematical and Physical Sciences, Graduate School of Natural Science and Technology, Kanazawa University, Kakuma, Kanazawa 920-1192, Japan

Received: May 25, 2007; In Final Form: July 30, 2007

The above-threshold dissociation of the ground state of a OH molecule under intense nonresonant laser pulses has been studied using the time-dependent Schrödinger equation with discrete variable representation. The applied field is assumed as a two-color mixed nonresonant laser pulses which has the nonresonant frequency ω and the overtone 2ω. After modulating the relative phase factor between the ω and 2ω pulse, we extracted a three-photon absorption peak or a five-photon absorption peak in the ATD spectrum.

1. Introduction

Since the advent of the laser technique, many physicists and chemists have developed several theoretical methods using laser pulses to gain deeper insight into the dynamical laser−molecule interaction. With an intense laser field, molecular systems show considerable changes in their electronic properties. The intense laser fields, with the intensity of $10^8 < I < 10^{12}$ W/cm^2, induce the multiphoton processes, such as multiphoton absorption, multiphoton ionization (MPI), and multiphoton dissociation (MPD),[1−3] which are fundamentally nonlinear optical processes arising from the higher-order effect of the external laser fields.[4]

Until now, theoretical developments with the laser pulse as an external field have been investigated by some approaches. The pump−dump scheme[5,6] was presented, in which the pump pulse first creates the wave packet on the excited potential energy surface (PES), and then, the dump pulse induces the stimulated transition to the desired state after an appropriate time delay. The π-pulse method, well-known in Fourier transform nuclear magnetic resonance (FT-NMR), was also applied to the population inversion of molecules. An optimal control theory (OCT) was proposed by Rabitz and colleagues[7,8] and shows the possibility to theoretically shape a highly effective pulse to control the molecule. Recently, Bergmann and coworkers[9−11] proposed the stimulated Raman adiabatic passage (STIRAP) method, a powerful technique to achieve the complete population transfer in molecular systems. This STIRAP method has been widely applied to control of the proton motion of the intramolecular hydrogen bond [12−15]and the isomerization reaction.[16,17] A number of generalizations of STIRAP have been proposed, including several intermediate states[18−20] and a continuum[21−23] for N-level systems. A similar method, known as adiabatic passage by light-induced potentials (APLIP),[24,25] uses the same counterintuitive pulse sequence as that of STIRAP. This method treats the vibrational motion of diatomic molecules explicitly and is a robust scheme particularly suitable for electronic transitions in diatomic molecules. The Raman chirped adiabatic passage (RCAP) has been proposed by combining STIRAP and a frequency-chirped pulse method[26,27] and is applied to induce the adiabatic transfer of a population in molecular vibrational ladders.

Now, we focus on the hydroxyl radical, OH, an important species in atmospheric chemistry and environmental chemistry. The dissociation and association processes of OH with multiphoton laser pulses were investigated by Korolkov et al.[28,29] These investigators used infrared (IR) subpicosecond pulses to transfer from the bound state into the continuum state through several bound vibrational states and proposed an efficient way of time-selective and space-selective control involving high-lying and dissociative states. Tran[23] also reported an alternative way of state-selective control via the continuum state. The Morse oscillator model of HeH^+ was applied to solving the TDSE with discrete variable representation (DVR) in his study. The generation of the highly vibrational excited state in the specified bond is an interesting problem in relation to the intramolecular vibrational relaxation (IVR) and the related bond dissociation.

In present study, we investigate multiphoton dissociation processes in the OH molecule by solving the DVR form of TDSE. The ground-state PES has the information for both bound vibrational and dissociative continuum states. Subsequently, all of the bound−bound, the bound−continuum, and the continuum−continuum transitions can be treated, and then, the above-threshold dissociation (ATD) spectra under intense laser pulses less than 10^{12} W/cm^2 can be found in the continuum region. First, the intense laser pulse, which has no resonant frequency with adjacent vibrational levels of the initial state, are used to obtain the ATD spectrum beyond the dissociation energy. The resultant spectrum has some peaks corresponding to multiphoton absorption from the initial state. Next, we try to realize coherent phase control of the ATD spectrum by using two-color mixed laser pulses. The frequency of the second laser pulse is defined by two photons $\omega_2 = 2\omega_1$, that is, overtone pulse for the first pulse frequency, ω_1. We then modulate the relative phase factor between the ω_1 pulse and the ω_2 pulse and discuss the phase dependency of the ATD spectrum.

† Part of the "Sheng Hsien Lin Festschrift".

* To whom correspondence should be addressed. E-mail: sugimori@kinjo.ac.jp.

‡ Kinjo University.

§ Kanazawa University.

10.1021/jp074071x CCC: $37.00
Published on Web 09/05/2007

2. Theoretical Treatments and Numerical Models

We treat the time-dependent Schrödinger equation (TDSE) within the Born−Oppenheimer approximation and the Morse oscillator model[30,31] for approximation of the electronic state. The unperturbed Hamiltonian of the molecule system is defined by

$$H_0(r) = T + V_M(r) \tag{1}$$

where T is the kinetic energy operator and V_M is the Morse potential energy operator given by

$$V_M(r) = D_e(1 - e^{-\alpha(r-r_e)})^2 \tag{2}$$

where r_e, D_e, and α are the equilibrium internuclear distance for the molecule, the dissociation energy, and the force constant, respectively. The parameters in the above Morse operator are calculated by fitting the $^2\Pi$ potential energy curve of the QCISD[32] calculation to the ground electronic state using the cc-pVTZ basis set of the Gaussian 03 package;[33] then, r_e = 1.7820 Bohr, $D_e = -37376.5$ cm^{-1}, and α = 1.3730 Bohr^{-1}.

The Morse oscillator can describe the well-defined potential energy curve of the diatomic molecule and has an analytical wave function to describe the vibrational state corresponding to the stretching vibration. The nth eigenvalue of the vibrational levels is given by

$$\epsilon_n = \omega_h\left(n + \frac{1}{2}\right) - x_e\omega_h\left(n + \frac{1}{2}\right)^2 \tag{3}$$

where ω_h and x_e are the harmonic frequency $\omega_h = (2\alpha^2 D_e/\mu_r)^{(1/2)}$ with the reduced mass μ_r of the OH molecule and the anharmonic constant $x_e = \alpha^2/2\mu_r\omega_h$, respectively. We find that there are 18 vibrational states in the Morse potential of the OH molecule by eq 3.

The time development of the molecular system can be described semiclassically by the TDSE

$$i\hbar\frac{d}{dt}|\Psi(t)\rangle = [H_0 + V(t)]|\Psi(t)\rangle \tag{4}$$

where H_0 is the molecular Hamiltonian, $V(t) = -\mu(r)\cdot\mathbf{E}(t)$ represents the interaction Hamiltonian between the classical electronic field $\mathbf{E}(t)$ and the molecular dipole moment function $\mu(r)$. In our simulation, the applied electric field $\mathbf{E}(t)$ is assumed as

$$\mathbf{E}(t) = E_1 g(t)\sin(\omega t) + E_2 g(t)\sin(2\omega t + \phi) \tag{5}$$

where E_1 and E_2 are the amplitudes of the electric field, ω is the pulse frequency, ϕ is a phase factor between the pulses, and the Gaussian shape function $g(t)$ is given by

$$g(t) = \exp\left[-\left(\frac{t - T_0}{\sigma}\right)^2\right] \tag{6}$$

where T_0 and σ are the temporal center and the pulse width of the Gaussian pulse, respectively; σ is fixed at 5 ps in this study. The above "two-color" laser pulses are adopted to control the energy distribution of the continuum state by modulating the phase factor ϕ.

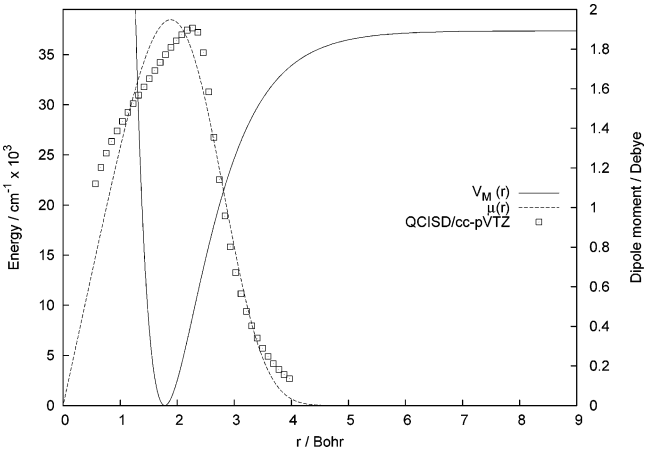

Figure 1. Morse potential curve $V_M(r)$ and dipole moment function $\mu(r)$. The QCISD/cc-pVTZ results of the dipole moment are also plotted.

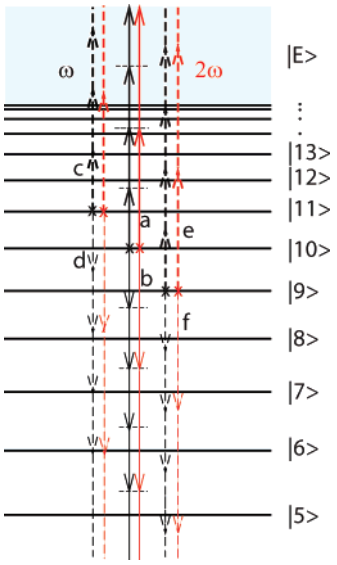

Figure 2. Pulse frequencies ω and 2ω of the applied laser pulse from the initial state $|10\rangle$ and energy levels around E_{10}. The applied frequency ω = 2633 cm^{-1} is not resonant with the nearest levels by $|10\rangle$, and multiphoton dissociation is achieved with more than three photons, 3ω, 4ω, ...

The population of the nth state vector $|\phi_n\rangle$ at time t is defined by integrating a squared value of the autocorrelation function

$$P_n(t) = |\langle\phi_n(r)|\Psi(r,t)\rangle|^2 = |C_n(t)|^2 \tag{7}$$

where $C_n(t)$ is the probability amplitude of the vibrational levels $|n\rangle$. The dissociation probability corresponding to the continuum state population is defined as

$$P_D(t) = 1 - \sum_n P_n(t) \tag{8}$$

and the continuum wave function is also defined by using each $C_n(t)$ and eigenvector

$$\Psi_{cont}(r,t) = \Psi(r,t) - \sum_n C_n(t)\phi_n(r) \tag{9}$$

When $\Psi_{cont}(r,t)$ reach the vicinity of r_{max}, their probability is dissipated gradually due to an absorbing potential.

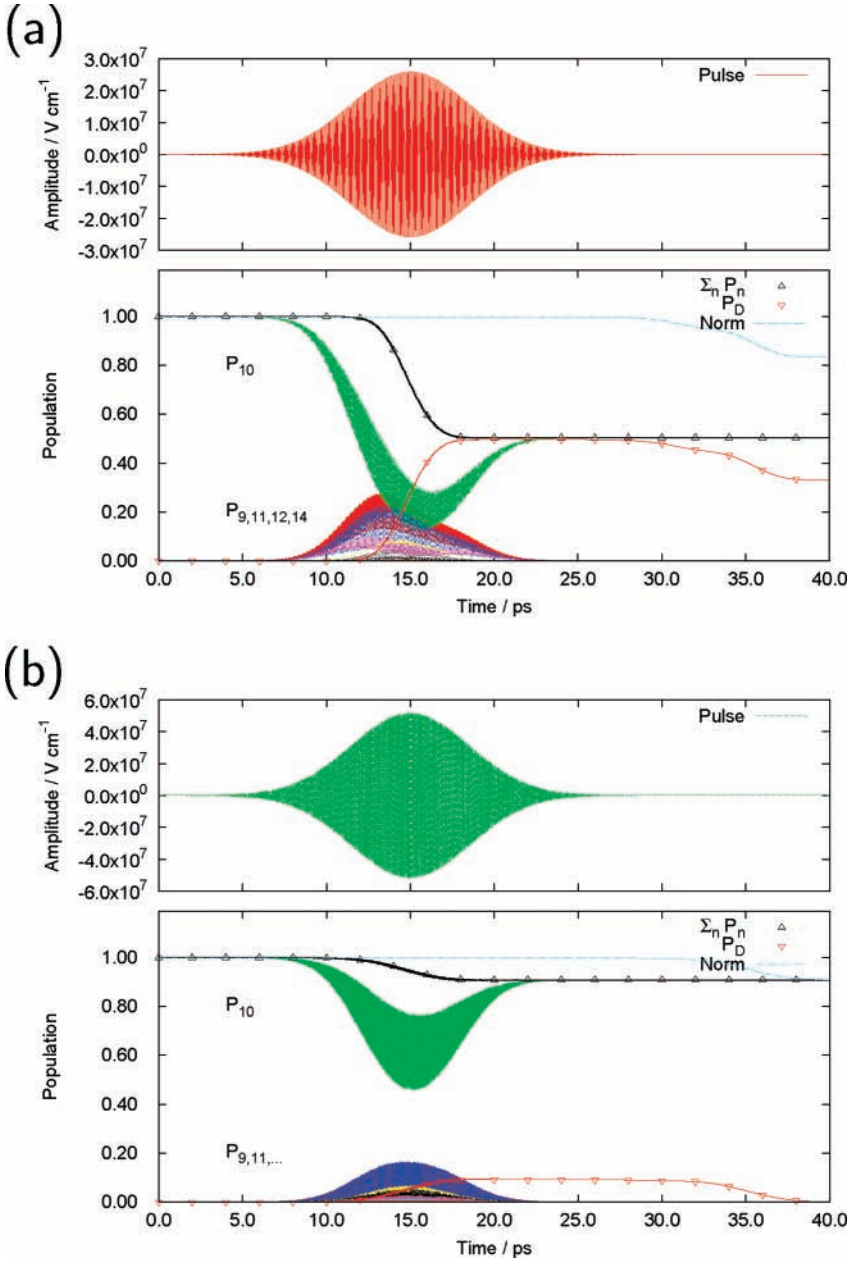

Figure 3. Pulse shape and population dynamics. (a) Pulse frequency ω with laser amplitude $E_1 = 2.0 \times 10^{-3}$ au and (b) overtone pulse frequency 2ω with $E_2 = 4.0 \times 10^{-3}$ au.

We employ the split-operator method[34,35] to solve the TDSE of the system numerically. The short-time propagator is approximated by

$$U(\Delta t) = e^{-iH\Delta t/\hbar} \approx e^{-iV\Delta t/2\hbar} e^{-iT\Delta t/\hbar} e^{-iV\Delta t/2\hbar} + O(\Delta t^3) \quad (10)$$

where the kinetic energy is given by the operator $T = p^2/2\mu_r$, and the potential term is $V(r,t) = V_M(r) + \mu(r)E(t)$. The dipole moment operator is approximated here by the following dipole moment function[36]

$$\mu(r) = \mu_0 x e^{-(x/x_0)^4} \quad (11)$$

where $\mu_0 = 0.522$ au/Bohr $= 0.205$ D/Bohr, and $x_0 = 2.67$ Bohr^{-1}, determined by fitting to QCISD/cc-pVTZ results, as shown in Figure 1.

The wave packet after time step Δt is explicitly estimated as follows by

$$\Psi(r,t_0 + \Delta t) = U(\Delta t)\Psi(r,t_0) = e^{-iV\Delta t/2\hbar} \mathrm{FFT}^{-1}[e^{-iT\Delta t/\hbar} \mathrm{FFT}\, [e^{-iV\Delta t/2\hbar}\Psi(r,t_0)]] \quad (12)$$

where FFT stands for the fast Fourier transform from the coordinate space to momentum space, while FFT^{-1} represents the inverse FFT from momentum to coordinate space. We set $\Delta t = 0.001$ ps and the initial wave packet $\Psi(r,0) = \phi_{10}(r)$ calculated by the 10th analytical eigenvector of the Morse oscillator. The spatial grid has a step size Δr of 0.01 Bohr, and the length of 655.36 Bohr is discretized by 65536 grid points.

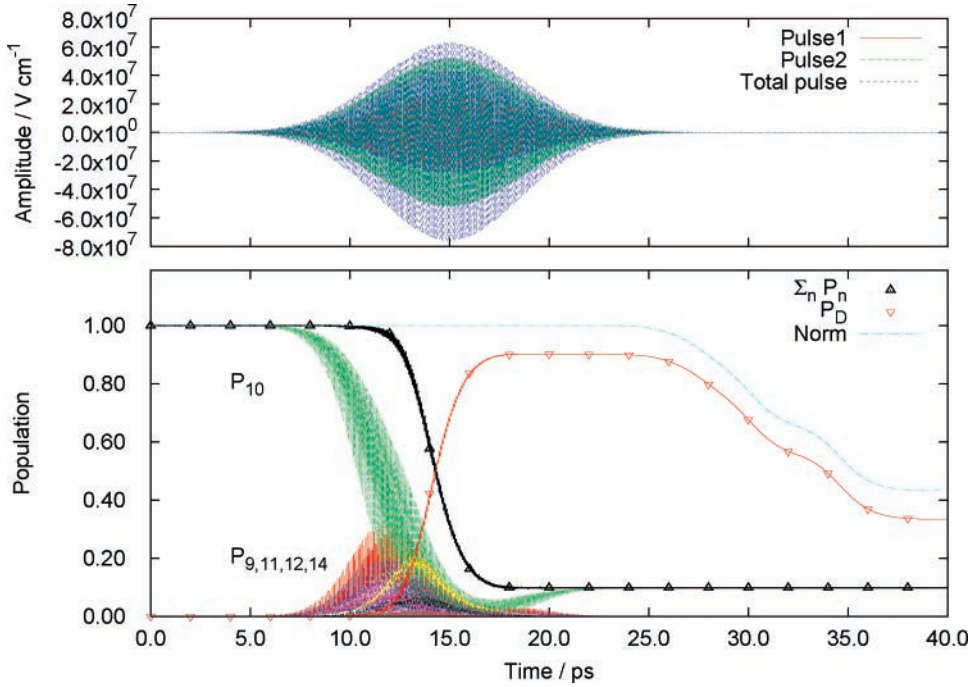

Figure 4. Pulse shape and population dynamics with two-color laser pulses $E(t)$, which have both laser parameters in Figure 3a and b. The phase factor $\phi = 0$.

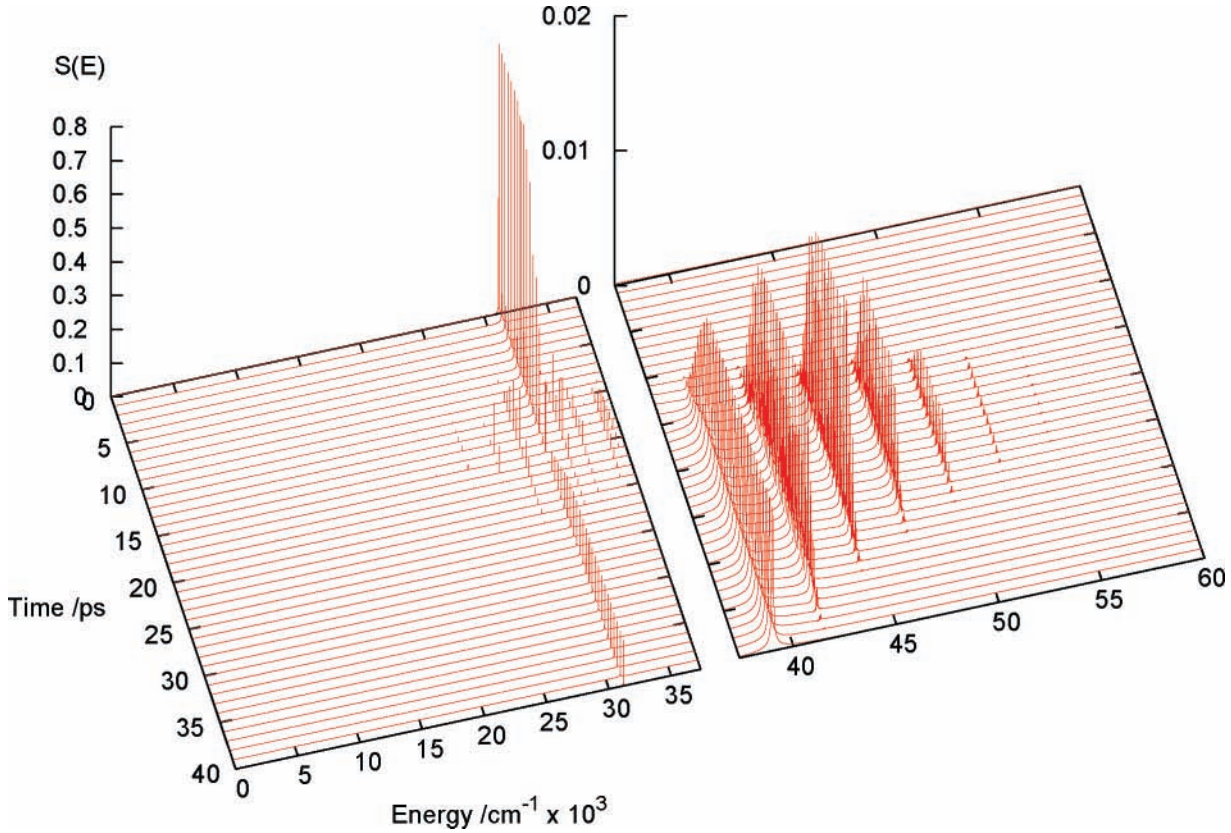

Figure 5. Time-dependent spectrum $S(E,t)$ with two-color mixed pulses of $\phi = 0$. The regions of the bound and the continuum states are separated at D_e, 37376 cm^{-1}.

To avoid an artificial reflection from the end point of the defined grid space, arbitrary imaginary absorbing potentials[37,38] are applied as follows

$$V^{abs}(r) = -ia \exp\left[-\left(\frac{r - r'}{\sigma'}\right)^2\right] \qquad (13)$$

where r' and σ' are the center position and width of the absorbing potential, respectively, and $a = 0.01$, $r' = 645.0$ Bohr, and $\sigma' = 5.0$ Bohr are used. When the continuum part of the wave function reaches the end point of the grid space, it gradually becomes dissipated, and the norm is not conserved in large-scale time propagation.

The continuum state of the resultant wave packet $\Psi_{cont}(t)$ is analyzed by the time-dependent spectrum method.[34,35,39] First, we perform the time development of an arbitrary wave packet $|\Psi(0)\rangle$, which includes some bound states of the Hamiltonian under consideration. We then calculate the autocorrelation function of the initial state $\Psi(t)$ and the time-developed state $\Psi(t+\tau)$. In the time development from t to T_0, the field-free Hamiltonian is applied without the absorbing potential V_{abs} to conserve the norm. Finally, we perform the Fourier transform of this autocorrelation function, which gives rise to the energy spectrum of the system. The following expression gives the mathematical foundation of this method

$$S(E,t) = \frac{1}{T}\int_0^T e^{iE\tau/\hbar}|\langle\Psi(t)|\Psi(t+\tau)\rangle|d\tau$$
$$= \sum_n |C_n(t)|^2 \frac{\hbar}{i(E-\epsilon_n)T}[e^{i(E-\epsilon_n)T/\hbar}-1] + \int dE'|C_{E'}(t)|^2\delta(E-E')$$
$$= \sum_n |C_n(t)|^2\delta(E-\epsilon_n) + \int dE'|C_{E'}(t)|^2\delta(E-E') \quad (T\rightarrow\infty) \quad (14)$$

where ϵ_n is the energy eigenvalue of the eigenstate $|n\rangle$ and $C_n(t) = \langle n|\Psi(t)\rangle$. If this spectrum method is applied to an arbitrary state, which is generated by the time development of any state under the strong laser pulse, then in addition to the energy spectrum of the bound states, the ATD spectrum comes out in a continuum energy region from the second term in eq 14 because the time-developed state $|\Psi(t)\rangle$ generally includes many bound states and continuum states due to the multiphoton absorption processes.

TABLE 1: Phase Dependency of Peak Intensities of ATD Spectrum $S(E > 37376\text{cm}^{-1}, t = 25\text{ ps})$

	peak intensity/arb. Unit					
phase ϕ/π	$S(E_{10}+3\omega)$	$S(E_{10}+4\omega)$	$S(E_{10}+5\omega)$	$S(E_{10}+6\omega)$	P_D	norm
0.00	0.02191	0.02392	0.02472	0.01425	0.850	0.993
0.25	0.01513	0.02290	0.02546	0.01323	0.893	0.992
0.50	0.02751	0.00959	0.01423	0.00597	0.895	0.996
0.75	0.03493	0.00617	0.00032	0.00084	0.901	0.999
1.00	0.02386	0.01936	0.01009	0.00047	0.856	0.999
1.25	0.01217	0.02196	0.02729	0.00255	0.635	0.999
1.50	0.01009	0.01544	0.01745	0.00334	0.386	0.999
1.75	0.01743	0.01056	0.02215	0.00854	0.634	0.988

3. Results and Discussions

In this section, we describe the results of the simulations, which aim to control the ATD spectrum. We have previously-realized the complete transfer from the vibrational ground state to the highly excited vibrational state by means of the STIRAP method.[40,41] The transition probability from the lower vibrational state to the continuum state is significantly small; therefore, in order to generate the continuum state due to ATD, it is effective to consider the relatively highly excited state as the initial state. In the following simulation, we adopted the $|10\rangle$ as the initial state.

3.1. One-Color Nonresonant Pulse. First, population transfer from the highly bound state $|10\rangle$ with a one-color nonresonant pulse is simulated to obtain the dissociation probability. Figure

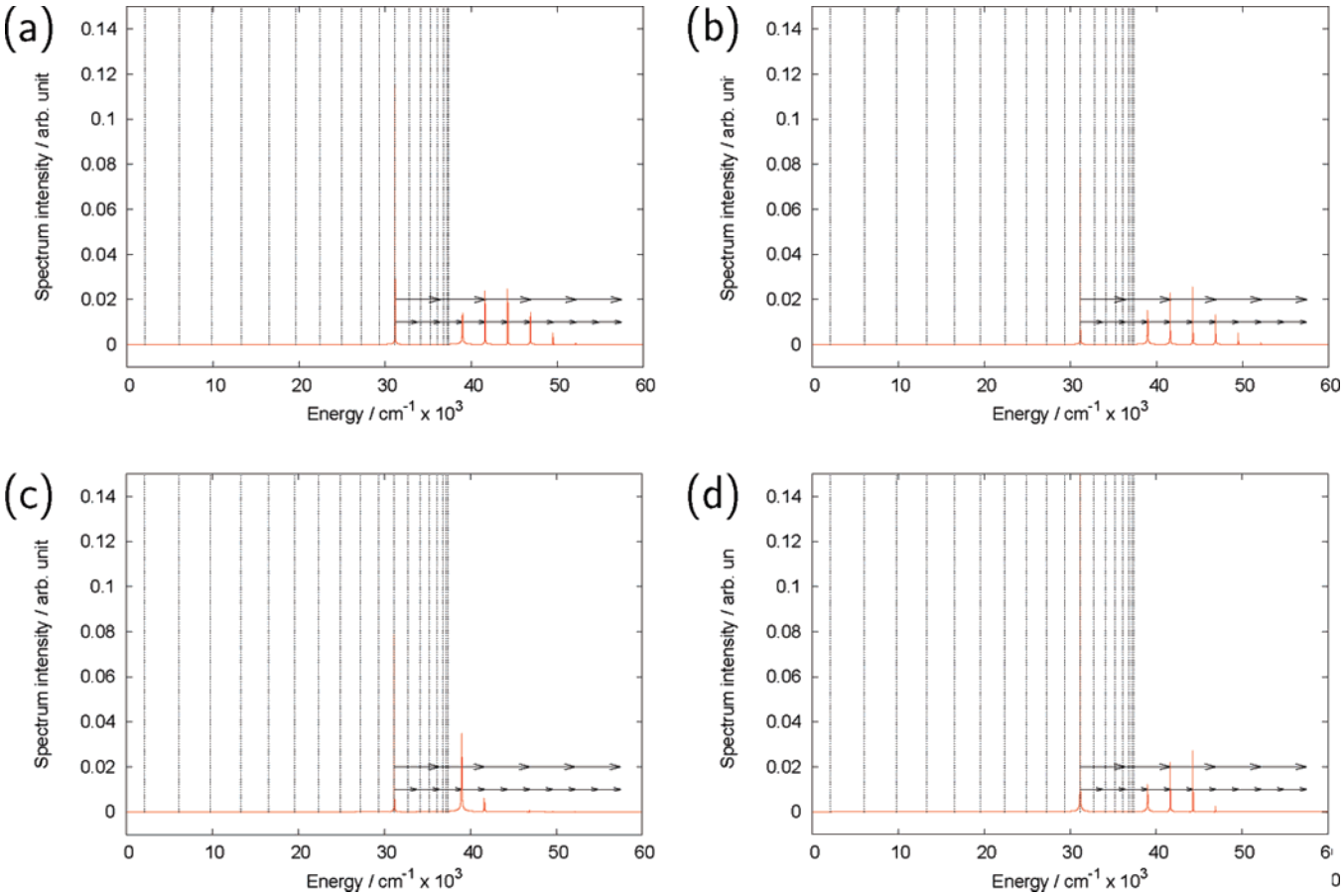

Figure 6. Time-dependent spectrum $S(E,t = 25.0\text{ ps})$ with two-color mixed pulses of various phase parameters. (a), (b), (c), and (d) denote results of $\phi = 0.0$, 0.25π, 0.75π, and 1.25π, respectively. Horizontal arrows represent photon energies of ω and 2ω.

2 shows energy levels of the bound state $|n\rangle$ and the pulse frequency ω as vertical arrows from $|10\rangle$, $|9\rangle$, and $|11\rangle$. Absorption and emission pathways are denoted as a, c, e and b, d, f, respectively. The applied pulse condition $\omega = 2633$ cm^{-1} is set to be nonresonant with the adjacent bound states, and more than three-photon absorption from $|10\rangle$ reaches the continuum state $|E\rangle$.

Before using two-color mixed pulses, each one-color pulse $E_1 g(t)$ sin (ωt) and $E_2 g(t)$ sin $(2\omega t)$ is tested. Figure 3 shows the pulse envelope in units of volts per centimeter and population dynamics for each bound state P_n, the total bound state population

$$\sum_n P_n$$

the dissociation probability P_D, and the norm of the wave packet. With a laser amplitude of $E_1 = 2.597 \times 10^7$ V/cm, P_{10} decreases, and P_D increases to 50% until 20 ps. The intermediates $P_{11,12,14}$ via the absorption pathways and the lower one P_9 via the emission pathways are shown in Figure 2. However, the absorption path a becomes the dominant process in the population transfer because no intermediates are generated after pulse irradiation. In Figure 3b, we show another result by using an overtone pulse frequency 2ω with a laser amplitude of $E_2 = 2E_1 = 5.194 \times 10^7$ V/cm,. Only overtone pulse irradiation leads to no significant changes such as a small dissociation probability and a small generation of intermediates.

3.2. Two-Color Mixed Nonresonant Pulses. Now, we present the results of two-color mixed laser-induced population transfer and analysis of the time-dependent spectrum. Figure 4 shows the pulse envelopes of two-color mixed nonresonant laser pulses defined by eq 5 and the population dynamics. The relative phase factor ϕ is fixed to 0.0 in this simulation. Because of overlapping two different pulses, the hypocritical pulse amplitude increases around the temporal center of the laser pulse, 15.0 ps. The dissociation probability then increases toward 85% quickly, while P_{10} decreases.

In order to obtain the energy distribution of the continuum state when the wave packet is dissociated, the time-dependent spectrum method is applied. The corresponding results at $t =$ 1, 2, ..., 40 ps are shown in Figure 5. We can see that the ATD spectrum of the continuum state ($E >$ 37,000 cm^{-1}) has several peaks due to multiphoton absorption from $|10\rangle$ under this pulse condition. However, high-energy peaks after 25.0 ps are dissipated because of the influence of the absorbing potential; thus, it means that the norm of the wave packet is not only conserved at the time period but also the dissipated peaks reach the terminal of the defined boundary. As a result, we find the spectrum peaks $S(E_{10} + 3\omega)$ arise from a direct bound−continuum transition between $|10\rangle$ and $|E\rangle$, and simultaneously, higher peaks than $S(E_{10} + 4\omega)$ are caused by both bound−continuum and continuum−continuum transitions.

3.3. Modulation of the Phase Factor. In the following subsection, we try to control such spectrum peaks by modulating the relative phase factor between the E_1 pulse and the E_2 pulse. The phase factor is set to be $\phi = 0.0$, 0.25π, 0.50π, 0.75π, 1.00π, 1.25π, 1.50π, and 1.75π. We note that the decrease of the norm leads to the disappearance of high-energy peaks of spectrum, and the spectrum is unstable during pulse irradiation. Thus, we analyze $\Psi(t = 25.0$ ps) by the time-dependent spectrum method. Table 1 shows peak intensities of the spectrum $S(E,t = 25$ ps) for various phase factors. We found the first peak $S(E_{10} + 3\omega)$ becomes the strongest when $\phi = 0.75\pi$, while the second and the third peaks increase when $\phi = 0.0$ and 0.25π.

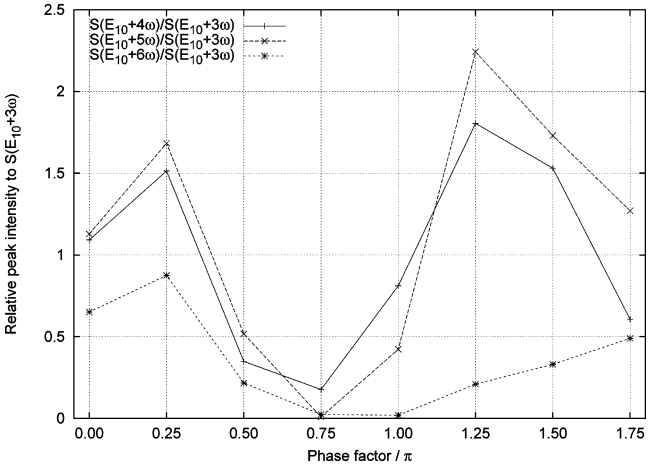

Figure 7. Phase dependency of relative peak intensities on $S(E_{10} + 3\omega)$, which are calculated from Table 1.

The results with $\phi = 1.25\pi$ and 1.50π have a rather little peak of the first peak. As shown in Figure 6, the relative peak intensities to $S(E_{10} + 3\omega)$ indicate such dependency on the phase clearly. The effect of the overtone pulse appears in the results with $\phi = 0.75\pi$ and 1.25π as the opposite way.

4. Concluding Remarks

In this study, we have investigated multiphoton dissociation from the highly excited vibrational levels of the ground state of OH with two-color mixed nonresonant pulses which have the nonresonant pulse frequency ω and the overtone 2ω. We have achieved above-threshold dissociation involved with more than three-photon absorption and have analyzed those spectra, including information of bound−bound, bound−continuum, and continuum−continuum transitions by using the time-dependent spectrum method.

We have also tried to control the spectrum peaks, for example, extraction of specific ATD peaks or elimination of any peak, with various phase factors between two laser pulses. As a result, $\phi = 0.25\pi$ and 1.25π have stressed three-photon and five-photon absorption in the ATD spectrum, respectively. For more detailed comparison, we should estimate the area of the peaks rather than the peak intensity. Although we can find the tendency due to phase control for ATD processes, additional work for optimizing pulse parameters is required based on the results.

Acknowledgment. H.N. is grateful for financial support from the Ministry of Education, Science and Culture of Japan (Research No. 19029014).

References and Notes

(1) Bucksbaum, P. H.; Zavriev, A.; Muller, H. G; Schumacher, D. W. *Phys. Rev. Lett.* **1990**, *64*, 1883.

(2) Giusti-Suzor, A.; He, X.; Atabek, O.; Mies, F. H. *Phys. Rev. Lett.* **1990**, *64*, 515.

(3) Magnier, S.; Persico, M.; Rahman, N. *J. Phys. Chem. A* **1999**, *103*, 10691.

(4) Hirschfelder, J. O., Wyatt, R. E., Coalson, R. D., Eds. *Lasers, Molecules, and Methods, Advances in Chemical Physics*; Wiley: New York, 1989; Vol. 73.

(5) Tannor, D. J.; Rice, S. A. *J. Chem. Phys.* **1985**, *83*, 5013.

(6) Tannor, D. J.; Kosloff, R.; Rice, S. A. *J. Chem. Phys.* **1985**, *85*, 5805.

(7) Shi, S.; Woody, A.; Rabitz, H. *J. Chem. Phys.* **1988**, *88*, 6870.

(8) Zhu, W.; Botina, J.; Rabitz, H. *J. Chem. Phys.* **1998**, *108*, 1953.

(9) Kuklinski, J. R.; Gaubatz, U.; Hioe, F. T.; Bergmann, K. *Phys. Rev.* **1989**, *40*, 6741.

(10) He, G.; Kuhn, A.; Schiemann, S.; Bergmann, K. *J. Opt. Soc. Am. B* **1990**, *7*, 1960.

(11) Bergmann, K.; Theuer, H.; Shore, B. W. *Rev. Mod. Phys.* **1998**, *70*, 1003.
(12) Ohta, Y.; Yoshimoto, T.; Nishikawa, K. *Chem. Phys. Lett.* **2000**, *316*, 551.
(13) Ohta, Y.; Bando, T.; Yoshimoto, T.; Nishi, K.; Nagao, H.; Nishikawa, K. *J. Phys. Chem. A* **2001**, *105*, 8031.
(14) Nishikawa, K.; Ohta, Y.; Yoshimoto, T.; Saito, T.; Nishi, K.; Nagao, H. *J. Mol. Struct.* **2002**, *615*, 13.
(15) Nishikawa, K.; Ito, T.; Sugimori, K.; Ohta, Y.; Nagao, H. *Int. J. Quantum Chem.* **2005**, *102*, 665.
(16) Shah, S. P.; Rice, S. A. *J. Chem. Phys.* **2000**, *113*, 6536.
(17) Kurkal, V.; Rice, S. A. *Chem. Phys. Lett.* **2001**, *344*, 125.
(18) Sola, I. R.; Malinovsky, V. S.; Tannor, D. J. *Phys. Rev. A* **1999**, *60*, 3081.
(19) Shah, S. P.; Tannor, D. J.; Rice, S. A. *Phys. Rev. A* **2002**, *66*, 033405.
(20) Sola, I. R.; Malinovsky, V. S. *Phys. Rev. A* **2003**, *68*, 013412.
(21) Carroll, C.; Hioe, F. T. *Phys. Rev. Lett.* **1992**, *68*, 3523.
(22) Nakajima, T.; Elk, M.; Zhang, J.; Lambropoulos, P. *Phys. Rev. A* **1994**, *50*, R913.
(23) Tran, P. *Phys. Rev. A* **1999**, *59*, 1444.
(24) Garraway, B. M.; Suominen, K.-A. *Phys. Rev. Lett.* **1998**, *80*, 932.
(25) Chang, B. Y.; Sola, I. R.; Santamaria, J.; Malinovsky, V. S.; Krause, J. L. *J. Chem. Phys.* **2001**, *114*, 8820.
(26) Chelkowski, S.; Gibbson, G. N. *Phys. Rev. A* **1995**, *52*, R3417.
(27) Regare, F.; Chelkowski, S.; Bandrauk, A. D. *Chem. Phys. Lett.* **2000**, *329*, 469.
(28) Korolkov, M. V.; Paramonov, G. K.; Schmidt, B. *J. Chem. Phys.* **1996**, *105*, 1862.
(29) Korolkov, M. V.; Manz, J.; Paramonov, G. K.; Schmidt, B. *Chem. Phys. Lett.* **1996**, *260*, 604.
(30) Morse, P. M.; Stueckelberg, E. C. G. *Phys. Rev.* **1929**, *33*, 932.
(31) Morse, P. M. *Phys. Rev.* **1929**, *34*, 57.
(32) Pople, J. A.; Head-Gordon, M.; Raghavachari, K. *J. Chem. Phys.* **1987**, *87*, 5968.
(33) Frisch, M. J.; Trucks, G. W.; Schlegel, H. B.; Scuseria, G. E.; Robb, M. A.; Cheeseman, J. R.; Montgomery, J. A., Jr.; Vreven, T.; Kudin, K. N.; Burant, J. C.; Millam, J. M.; Iyengar, S. S.; Tomasi, J.; Barone, V.; Mennucci, B.; Cossi, M.; Scalmani, G.; Rega, N.; Petersson, G. A.; Nakatsuji, H.; Hada, M.; Ehara, M.; Toyota, K.; Fukuda, R.; Hasegawa, J.; Ishida, M.; Nakajima, T.; Honda, Y.; Kitao, O.; Nakai, H.; Klene, M.; Li, X.; Knox, J. E.; Hratchian, H. P.; Cross, J. B.; Bakken, V.; Adamo, C.; Jaramillo, J.; Gomperts, R.; Stratmann, R. E.; Yazyev, O.; Austin, A. J.; Cammi, R.; Pomelli, C.; Ochterski, J. W.; Ayala, P. Y.; Morokuma, K.; Voth, G. A.; Salvador, P.; Dannenberg, J. J.; Zakrzewski, V. G.; Dapprich, S.; Daniels, A. D.; Strain, M. C.; Farkas, O.; Malick, D. K.; Rabuck, A. D.; Raghavachari, K.; Foresman, J. B.; Ortiz, J. V.; Cui, Q.; Baboul, A. G.; Clifford, S.; Cioslowski, J.; Stefanov, B. B.; Liu, G.; Liashenko, A.; Piskorz, P.; Komaromi, I.; Martin, R. L.; Fox, D. J.; Keith, T.; Al-Laham, M. A.; Peng, C. Y.; Nanayakkara, A.; Challacombe, M.; Gill, P. M. W.; Johnson, B.; Chen, W.; Wong, M. W.; Gonzalez, C.; Pople, J. A. *Gaussian 03*, revision B.05; Gaussian, Inc.: Wallingford, CT, 2004.
(34) Feit, M. D.; Fleck, J. A.; Steiger, A. *J. Comput. Phys.* **1982**, *47*, 412.
(35) Feit, M. D.; Felck, J. J. A. *J. Chem. Phys.* **1983**, *78*, 301.
(36) Sugawara, M.; Fujimura, Y. *Chem. Phys.* **1995**, *196*, 113.
(37) Leforestier, C.; Wyatt, R. E. *J. Chem. Phys.* **1983**, *78*, 2334.
(38) Bisseling, R. H.; Kosloff, R.; Manz, J. *J. Chem. Phys.* **1985**, *83*, 993.
(39) Dai, J.; Zhang, J. Z. H. *J. Chem. Phys.* **1995**, *103*, 1491.
(40) Ohta, Y.; Yoshimoto, T.; Nishikawa, K. *Nolinear Optics* **2000**, *26*, 137.
(41) Sugimori, K.; Ito, T.; Nagao, H.; Nishikawa, K. *Int. J. Quantum Chem.* **2005**, *105*, 596.